Physical Review & Research International
3(4): 642-665, 2013

SCIENCEDOMAIN *international*
www.sciencedomain.org

Spectral and Relaxation Properties of the Photoconductivity of Thin TiO_2 Films Produced by the Sol-gel Technique

V. I. Bredikhin[1*], V. N. Burenina[1], Yu. A. Mamayev[1] and S. N. Yashin[1]

[1]Institute of Applied Physics, Russian Academy of Sciences, 46 Ulyanov st. Nyzhnii Novgorod, 603950, Russia.

Authors' contributions

This work was carried out in collaboration between all authors. All authors read and approved the final manuscript.

Research Article

Received 30th March 2013
Accepted 29th June 2013
Published 3rd August 2013

ABSTRACT

Photoconductivity of TiO_2 thin films is investigated in experiment. The excitation is performed by both a continuous Hg quartz lamp and laser sources. The photoconductivity kinetics and spectrum are investigated. The multi relaxation character of photoconductivity kinetics is revealed. The photoconductivity spectrum is measured in the 250 ÷ 420 nm range. The nature of the observed features is discussed.

Keywords: Thin films; titania; photoconductivity; relaxation properties; photoconductivity spectrum.

1. INTRODUCTION

Titanium dioxide TiO_2 (titania) is challenging to researchers in diverse fields of science that seem to be absolutely independent at first sight. This is due to a number of reasons. First, high stability of the properties specified by higher chemical durability as compared to other transition metals oxides. Second, TiO_2 band-gap energy corresponds to the near UV range, which permits using the radiation of gas-discharge lamps for excitation of current carriers in the samples. In addition, by doping the film it is possible to shift its absorption spectrum to the visible region.

[*]Corresponding author: Email: bredikh@appl.sci-nnov.ru;

Titania films possess high catalytic activity and may be used as self-cleaning [1] or anti-bacterial coatings [2,3], and as elements for hydrogen energetics [4]. Also, TiO_2 films possess unique surface properties that allow producing coatings for windowpanes and for the technologies based on superhydrophilicity, when liquids are distributed over the surface without drop formation [5]. TiO_2 films change their conductivity when gas molecules are adsorbed on their surface; this property is useful for creating sensors [6]. TiO_2 films may be used for elaborating solar-blind UV photoreceivers that do not react to visible light. Thus, a thin TiO_2 film is a promising material for many nanotechnologies.

Many unique properties of TiO_2 films enumerated above become apparent under the action of UV radiation, which is evidently associated with free charge generation, hence, with the photoconductivity effect. Therefore, study of TiO_2 film photoconductivity is important for understanding many phenomena and their applications and quite a number of publications were devoted to this problem. For example, the photoconductivity effect for TiO_2 films obtained by the sol-gel technique was described in the paper [7]. The conductivity in the dark and under Xenon lamp illumination was measured in ambient air and in vacuum. It was shown that the onset of photocurrent depends on time with character rise and relaxation times from tens to thousands of seconds, but no analysis was made. The photoconductivity of TiO_2 films produced by magnetron sputtering was investigated theoretically and experimentally in [8]. The experiments demonstrated a variety of time dependences of photoconductivity onset. Typical times of the processes are the same as in [7]. A theoretical model based on the concept of two types of traps was proposed for description of the experimental data. The authors of [9] described the experiment in which charge carriers were excited under the action of a femtosecond laser pulse and photoconductivity was observed by means of terahertz spectroscopy. In those experiments photoconductivity pulses (free charge concentration) were measured by the variation of the reflection coefficient of terahertz electromagnetic radiation. Photoconductivity relaxation times were assessed to be from tens to hundreds of picoseconds.

The impact of different admixtures and phase structure on the absorption edge shift and the corresponding photoconductivity shift to the visible region was considered in [10,11]. However, there is still no comprehensive picture of the origin of photoconductivity in TiO_2. For example, strict correlation between the magnitude and character of photoconductivity and the technology of film production and their structure has not been verified yet, relaxation features of photocurrent have not been investigated, there is no data on photoconductivity spectrum.

It is worth noting that TiO_2 occurs in Nature in several states differing by the crystal lattice structure: brookite, anatase and rutile. TiO_2 films freshly deposited by the sol-gel technique are amorphous after drying, consist primarily of brookite after heat treatment up to~ 300 ºC, then anatase is observed in ~ 250 ÷ 700 ºC range of heat treatment, and the brookite phase is in the ~500 ÷ 900 ºC range of heat treatment [12]. For many applications [1-4] (for our experiments, in particular) the film should be in the anatase phase. The ratio of different phases in samples strongly depends on the technology and conditions of fabrication. For example, with magnetron sputtering or gas phase deposition film temperature is high in the beginning which results in high concentration of routile. The sol-gel technology allows thermal treatment of the deposited films in an arbitrary temperature regime and control of film composition [13-15].

On the other hand, it is known that the photoelectric and catalization properties of films obtained by different methods differ essentially. The physico-chemical causes of this difference have not been fully understood.

The goal of this work is investigation of the photoconductivity effect in different experimental samples (TiO_2 films of different thickness and phase composition) obtained by the sol-gel technique, that has a number of obvious advantages, and study of the relaxation and spectral properties of photoconductivity of TiO_2 films.

2. EXPERIMENTAL SAMPLES

There are different methods of deposition of thin, transparent film materials, TiO_2 in particular. Sputtering is the technique most frequently used in industries for depositing films of any composition on large areas. A film is formed on a substrate by sputtering a target material when the surface of the target is bombarded by ions of operating gas (usually argon) that are formed in a glow discharge plasma [16]. This technique is highly flexible in controlling the process of single layer deposition. It allows depositing gradient films and forming nonequilibrium composites. It is a high-tech method that demands complex and expensive equipment.

An alternative method is chemical vapor deposition when a solid film is formed under the action of chemical reactions from a material in gaseous or plasma state [17]. Both these methods are rather complicated and demand complex and expensive equipment, especially for obtaining large-area films.

In the present work we study the properties of mesoporous films [13] produced by the sol-gel technique [14,15]. TiO_2 films were deposited by the chemical method from solutions of hydrolyzed compounds (the sol-gel technique). 5% tetrabutoxytitanium $Ti(OC_4H_9)_4$ in isopropyl alcohol was used as a film-forming agent. Hydrochloric acid served as a catalyst and a stabilizer. The solution was centrifuged on the surface of a molybdenum or silica glass substrate to form a transparent layer of polymerized titanium acid of uniform thickness. On evaporation, we obtained a transparent TiO_2 film firmly bound to the glass surface. The advantages of this method are its relative simplicity and no need of complex and expensive equipment. Still another significant advantage is that the sol-gel technique enables depositing films on surfaces of arbitrary large area.

As our research concerns, primarily, films possessing anatase structure, we annealed them at a temperature up to 520 ºC. However, as a rule films are not fully converted to anatase and the obtained samples have rutile inclusions embedded in the anatase matrix [18].

We investigated samples produced by different techniques:

1. TiO_2 film freshly deposited and dried at a temperature up to 100 °C; thickness ~80 nm, substrate – glass (sample 1).
2. Film annealed after drying at ~450 °C; thickness ~40 nm, substrate – glass (sample 2).
3. Film annealed at ~450 °C; thickness ~80 nm, substrate – glass (sample 3).
4. Film about 80 nm thick deposited on a quartz glass substrate and annealed at ~450 °C (sample 4).
5. Half the film of sample 4 re-annealed at 520 °C (sample 5).

The 40 nm films consisted of a single layer, and the 80 nm films comprised two layers each of which was dried and annealed separately.

The thickness of the samples was measured by the ellipsometric method. The index of refraction of the annealed films was 2.2 – 2.28. By comparing the obtained index of refraction of the film with that of anatase single crystal $n_D \approx 2.488$ [19], we estimated the volume porosity of the films to be ≈ 13%. According to the AFM measurements, the pore diameter did not exceed 10 ÷ 20 nm.

3. FILM TRANSMISSION SPECTRA

The transmission spectra of TiO_2 films obtained with the UVI spectrophotometer SF-256 (Russia) with allowance for background substrate transmission are presented in Fig. 1a. Clearly, the films absorb the near ultraviolet light and are transparent for the visible and infrared range (the sinusoidal structure of the spectrum in the transparency region is associated with interference in a thin film), which agrees with the results reported in other papers and studies.

By transmission spectra of films one can calculate the forbidden gap of a semiconductor. To do so, it is necessary to plot squared absorption coefficient (TiO_2 is supposed to be a direct-gap semiconductor) versus frequency (in energy units), and extrapolate the linear part of this dependence by a straight line up to the intersection with the frequency axis; the point of intersection with the frequency axis is the forbidden gap (Fig. 1b and Fig. 1c). The forbidden gap for the annealed film varies within the 3.7 ÷ 3.8 eV interval. The spread in the values may be due to inaccurate measurements, e.g., difficulty of taking into account interference in the film, or to spread in the film properties.

4. STUDY OF THE PHOTOCONDUCTIVITY EFFECT IN EXPERIMENTAL SAMPLES

Photocurrent was excited in the sample under the action of mercury-discharge lamp PRK-4 (Russia). The photocurrent was measured by means of a digital oscillscope RIGOL DS1052E. The schematic of the experimental setup is shown in Fig. 2.

The experimental sample was a glass substrate with a film on the surface of which electrodes are glued with a conductive silver adhesive. The electrode size and geometry are given in Fig. 2. The distance between the electrodes was chosen to be about 5 mm as this size allows focusing radiation of the lamp and, at the same time, excluding exposure of the electrodes to light, thus reducing spurious photoconductivity.

The test measurements showed that, with the parameters used in our work, the photoelectric response depended linearly on the applied voltage and illumination. The response time at voltage switching on and off was determined by the external circuit time constant, which indicated that that the electrode-film contacts were ohmic.

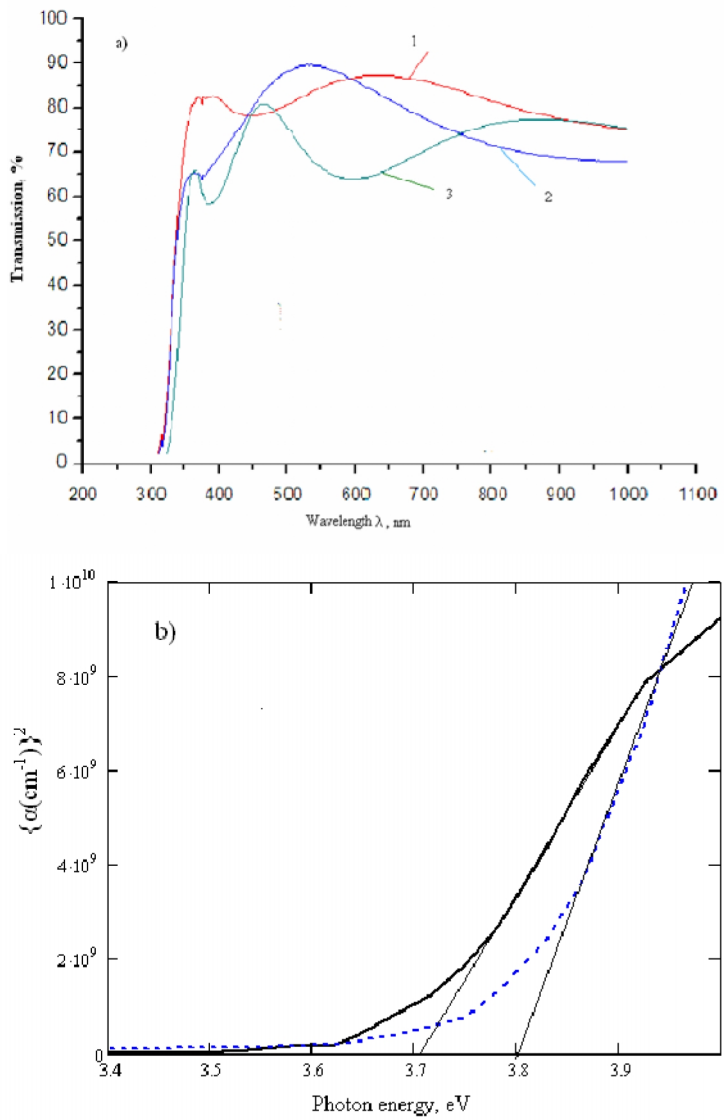

Fig. 1. a) Transmission spectra of samples; curve 1 is for sample 1, curve 2 is for sample 2, curve 3 is for sample 4.; b) plot for determining annealed film forbidden gap

During the experiments we surveyed processes of the onset of photoconductivity in the sample under the action of a light source and studied the influence of different sections of the lamp spectrum on photoconductivity (in some experiments different light filters, including UVL-1(Russia) that fully cuts off the visible portion of the spectrum, were placed between the sample and the lamp) or diffraction monochromator MDR 2 for extracting separate lines of PRK-4 lamp radiation. Besides, we investigated relaxation processes at “short” times, for which the radiation was switched on or off for a short time period by means of an optomechanical shutter. The power of UV radiation incident on the interelectrode space and measured by the optical power meter IMO-2M was up to 23 mW in the total spectrum and up to 7 mW in the UV spectrum extracted by the filter UVL-1.

We carried out test experiments to make sure that the observed photoconductivity was associated with the photoconductivity of the film rather that of the glass that also absorbs light in the UV region or of air ionized by light from a lamp. We measured the photoconductivity signal on the electrodes deposited on bare glass illuminated by a lamp. No photoconductivity was observed in those experiments.

In the first series of experiments a sample was first illuminated by a lamp (with the power supply on) until the signal on the oscilloscope screen attained a stationary or maximum value. After that the light source was switched off and photoconductivity relaxation was watched on the oscilloscope screen. Data on the oscilloscope were stored and processed on a computer.

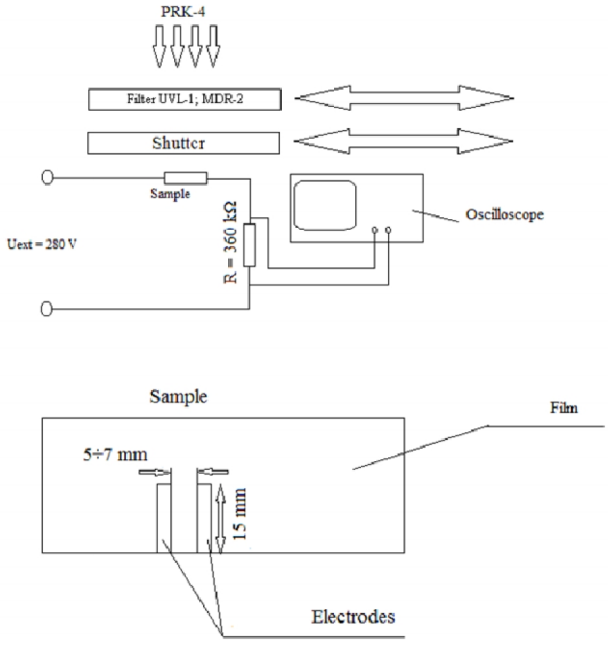

Fig. 2. Schematic of photoconductivity measurements.

The most pronounced photoconductivity effect was obtained in the experiments with samples 3 and 4. A section of the experimental oscillogram and the result of processing – plots of photocurrent density versus time – are shown in Figs. 3,4. Repeated measurements gave identical results.

In the experiment with sample 1 the photoconductivity effect was insignificant. The signal on the oscilloscope screen was weak not only in comparison with samples 3,4, but barely visible against the background of power source noise (Fig. 5).

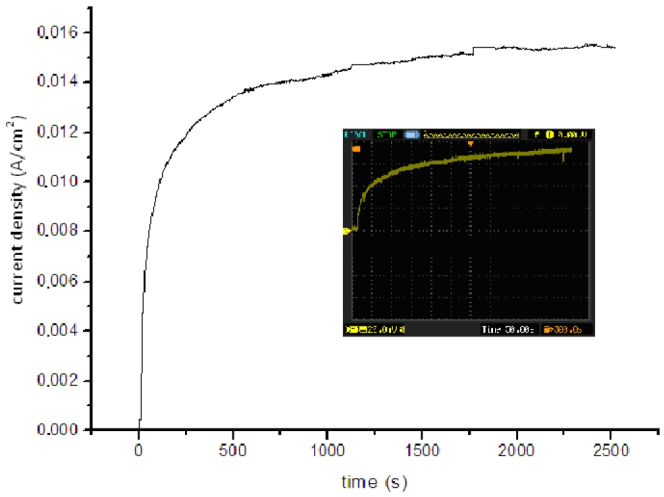

Fig. 3. Sample 3, time dependence of current density at constant illumination of the sample. The light is on. Inset: oscillogram of the signal

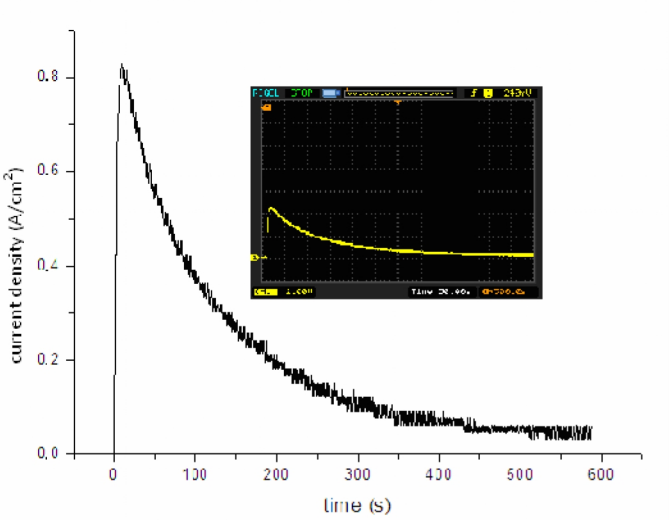

Fig. 4. Current density versus time in sample 4 under continuous illumination. The light is on. Inset: signal oscillogram

An interesting result was obtained in the experiment with sample 2. When the sample was exposed to light, a small photoconductivity effect was observed, but in about a minute the photocurrent dropped down to zero (Fig. 6), although illumination was continued. The effect was repeated after cleaning the sample surface by alcohol with the same result. The photoconductivity always relaxed in a short time despite the continued illumination. The conductivity in this sample was most likely connected with surface activity (or with photochemical decomposition of organic admixtures in alcohol), and the contribution to the photoconductivity of the carriers excited in the film thickness was insignificant because the film was rather thin.

The photoconductivity effect in sample 5 was much weaker than in sample 4, the photocurrent in the sample built up very slowly and relaxed for a long time as well (see Fig. 7).

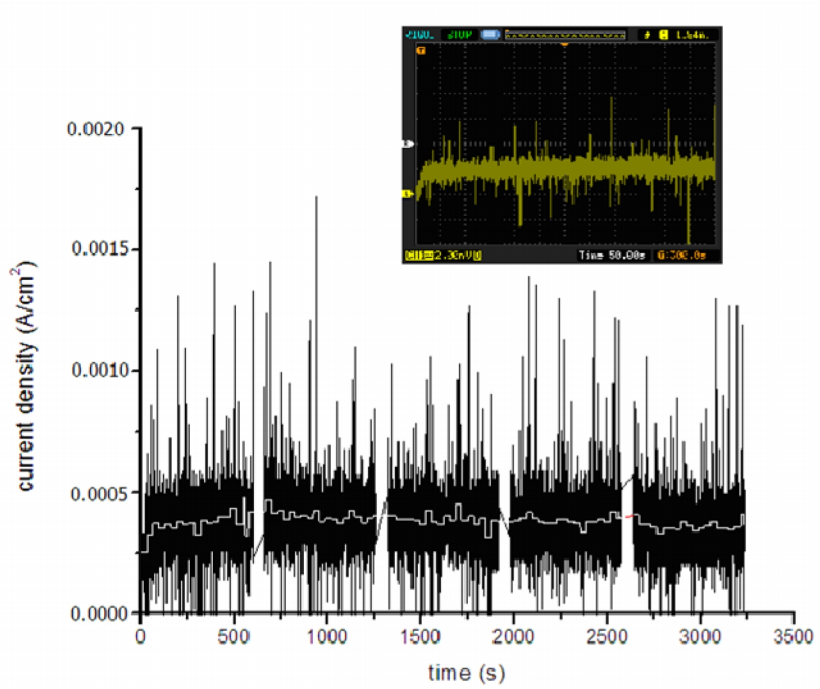

Fig. 5. Current density versus time in sample 1 under continuous illumination. The light is on. Useful signal against the background of noise is shown by light color. Inset: signal oscillogram

Fig. 6. Oscillogram of the signal in sample 2. The light is on

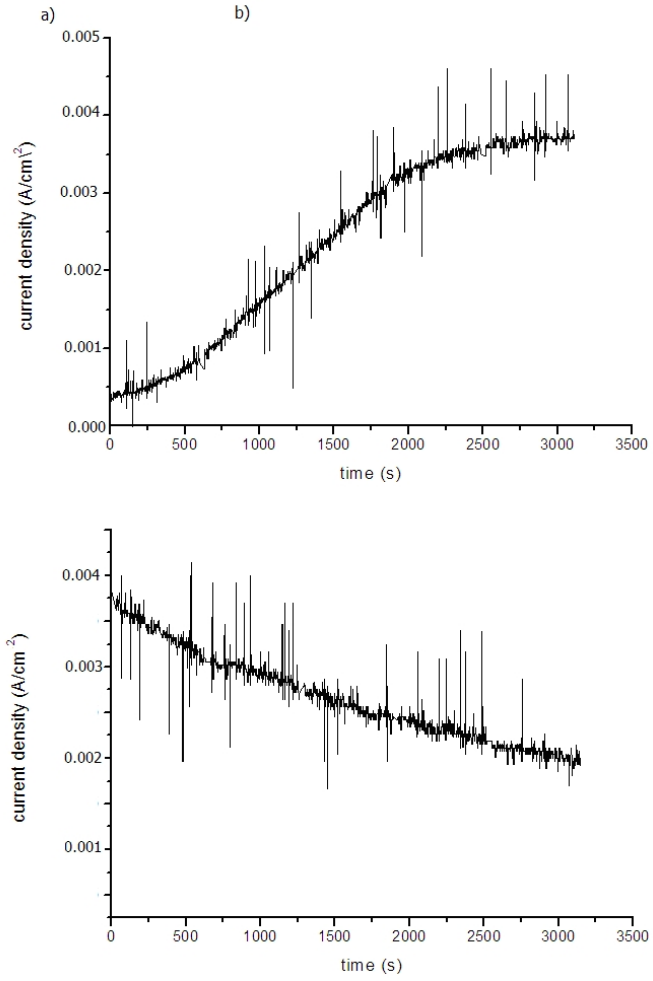

Fig. 7. Sample 5: a) photocurrent buildup under continuous illumination (The light is on.), b) photocurrent relaxation after the illumination (The light is off)

4.2 Study of Relaxation Processes in Experimental Samples

Photocurrent relaxation times bear important information on electron structure of the film. Therefore, a substantial part of the work is concerned with this aspect of the phenomenon.

The process of photocurrent buildup in sample 3 under the action of full spectrum lighting and relaxation is approximated in Fig. 8. From physical considerations it is clear that the photoconductivity kinetics is determined by the relaxation processes described by exponential dependences. An example of the relaxation description of photoconductivity in TiO_2 films is given, e.g., in [8]. However, the processes observed in the current work are not described by a single relaxation process. Hence, it is natural to seek a polyrelaxation description in which several (two or more) relaxation process with markedly differing time

constants occur. Hence, the process is approximated here by the function for photocurrent buildup under illumination of the form

$$f_1 = A_1(1 - e^{-\frac{t}{\tau_1}}) + A_2(1 - e^{-\frac{t}{\tau_2}}) \quad (1)$$

and by the function for relaxation of the form

$$f_2 = A_3(e^{-\frac{t}{\tau_3}}) + A_4(e^{-\frac{t}{\tau_4}}) \quad (2)$$

For the data in Fig. 8a, the times of signal buildup are τ_1 = 625 s; τ_2 = 72 s
For the data in Fig. 8b, the times of signal buildup are τ_3 = 72 s; τ_4 = 7 s

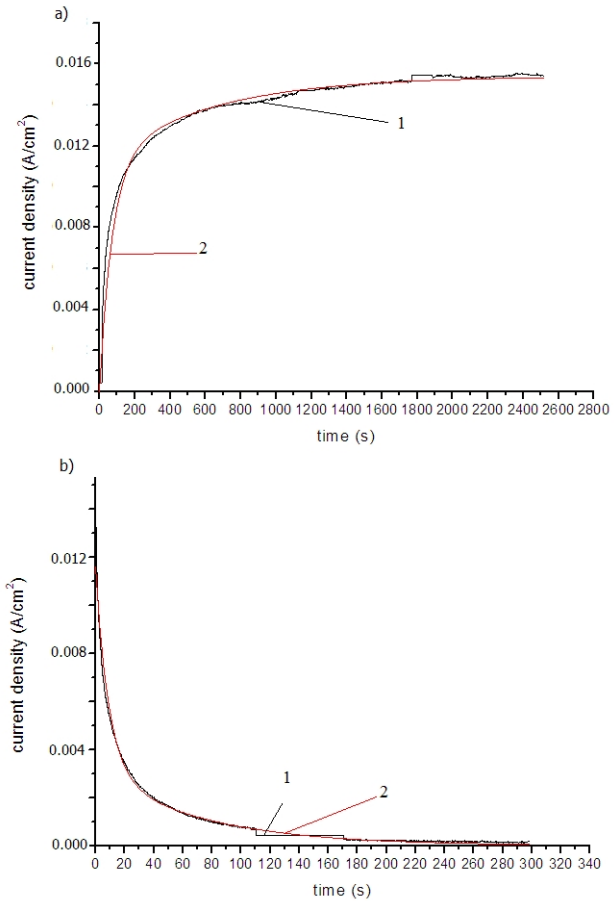

Fig. 8. a) Photocurrent buildup in sample 3 (the light is on), b) photocurrent relaxation in sample 3 (the light is off); curves 1 are experimental, red (color on-line) curves 2 are the approximating data

An analogous experiment was conducted with UVL-1 filter. The relaxation and buildup times in that experiment coincided with the previous ones.

Functions (1) and (2) represent phenomenological description of the observed process of photocurrent buildup and relaxation. The authors of [9] approximated the decaying parts of the photoconductivity pulses by the function of the form (2), but they spoke about times of order tens and hundreds of picoseconds.

Thus, by monitoring the photocurrent buildup and relaxation it is possible to determine characteristic relaxation times of the processes running in the film. Besides, one can readily see that these times markedly differ from each other. Relaxation processes in the film may evidently occur with times smaller than τ_4, but to detect them it is necessary to consider a process with the corresponding time scale (the times ≤ 10^{-10} s were obtained in the work ([9]).

To clarify the relations (1) and (2) and find faster relaxation times we conducted the following series of experiments. A sample was first illuminated by a lamp until photocurrent attained a noticeable value. After that the lamp was shuttered off and the signal on the oscilloscope screen started to relax, and then the lamp was switched on again but only for fractions of a second (0.5 s, 0.25 s and 0.14 s) which was controlled by the optomechanical shutter. The oscillograms of the photoconductivity pulses observed in the experiment and recalculated to current density are shown in Fig. 9 for different times T of sample exposure. The experiment was carried out with and without UFL-1 filter.

The fronts of the building up parts of the photoconductivity pulses in sample 3 are approximated in Fig. 10. The function of the form (1) persists to be the approximating function, but the characteristic times in the exponents are shorter.

The characteristic times: τ_1 = 0.2 s; τ_2 = 0.02 s.

The relaxation parts of photocurrent pulses may be approximated analogously (see Fig. 11). Characteristic relaxation times: τ_4 = 0.2 s; τ_3 = 7 s.

From the data in Figs. 10, 11 it is clear that in the experiments with and without UFL-1 filter the characteristic times of relaxation processes coincide. Hence, the visible light that is cut off by the filter does not affect dynamics of the charge carriers excited in the film.

The process is more complicated in sample 4. Under constant illumination the photocurrent has a maximum after which it starts to decay. The two branches have different relaxation times. Moreover, when illumination is switched off, the photocurrent relaxes with its own times that are close to the times at which the photocurrent starts to buildup when illumination is switched on. The parts of photocurrent buildup and relaxation and the process of photocurrent relaxation when illumination is switched off are approximated in Fig. 12.

For the building up part of photocurrent and for the relaxation after the lamp is switched off the characteristic times of relaxation processes are: $\tau_1 = \tau_3$ =2.3 s; $\tau_2 = \tau_4$ = 0.02 s.

The characteristic times of relaxation processes determined by the relaxation part of the time dependence (the lamp is not switched off) of photocurrent are the following: τ_5 = 600 s; τ_6 = 90 s.

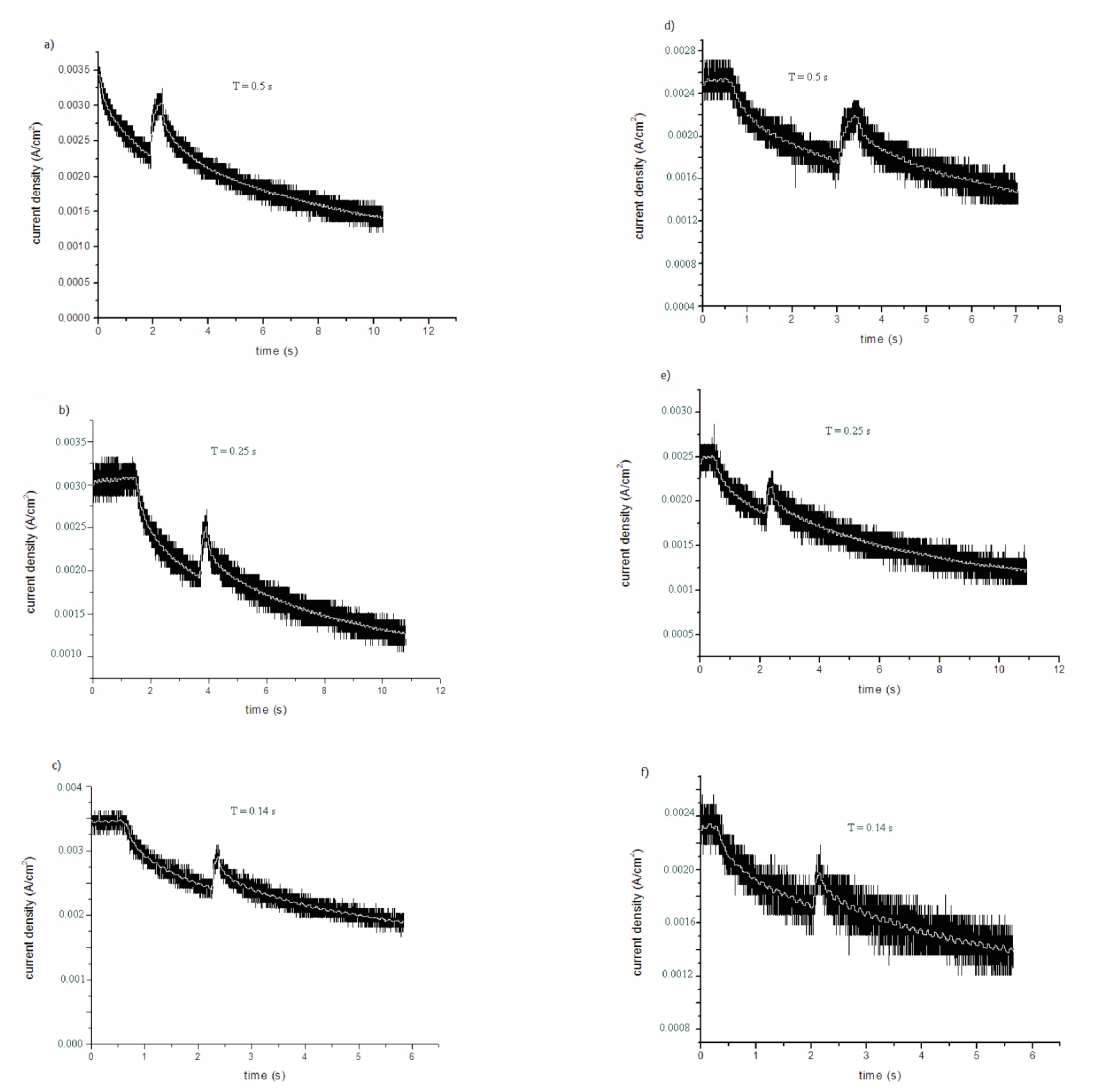

Fig. 9. Photoconductivity pulses in sample 3 (the light is on for short time). Useful signal against the background of noise is shown by light color. a), b), c) pulses without filter; d), e), f) pulses with UFL-1 filter

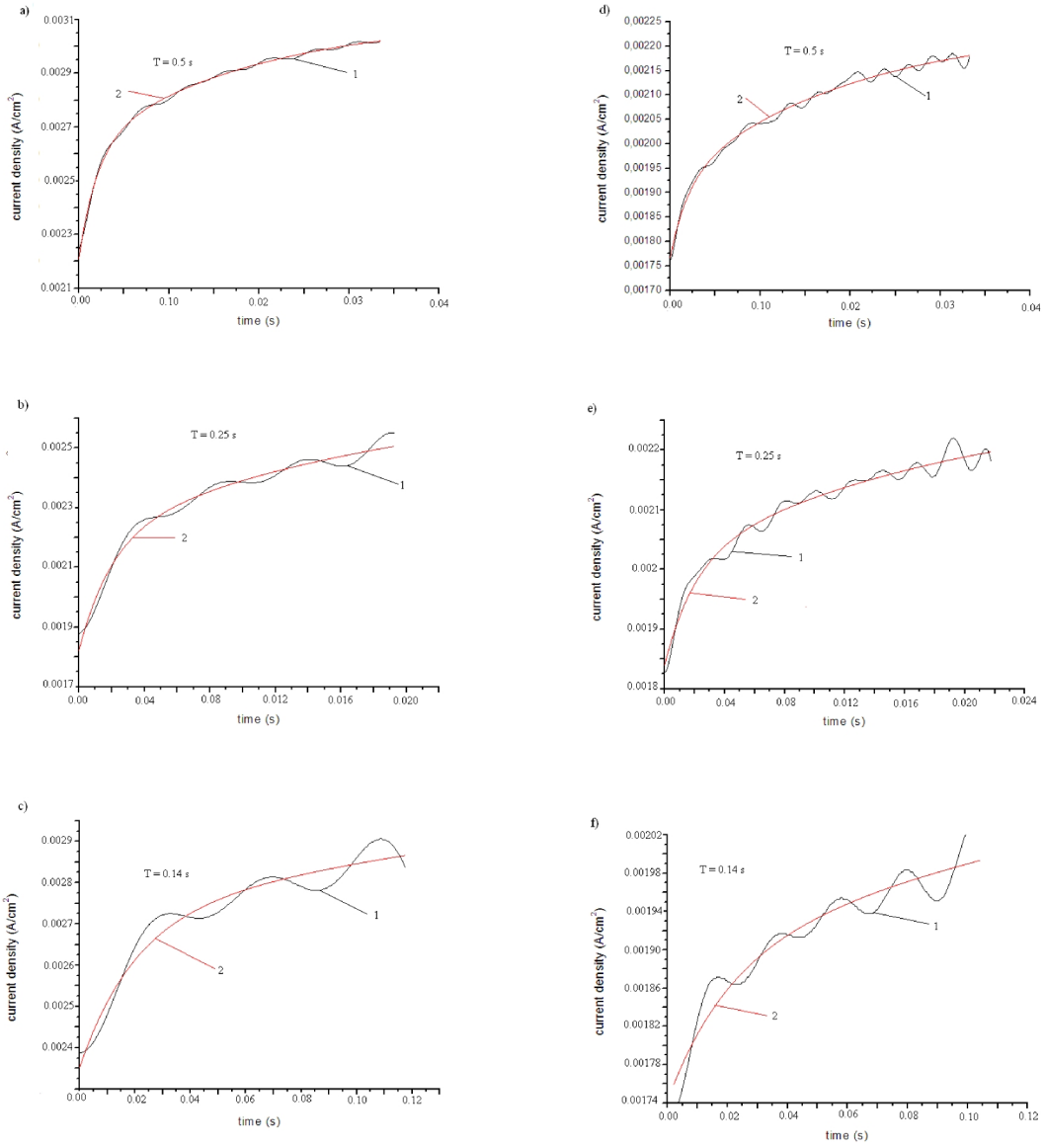

Fig. 10. Approximation of building up parts of photocurrent pulses in sample 3 (the light is on): a), b), c) experiment without filter; d), e), f) experiment with UVL-1 filter. Curves 1 are experimental, red (color on-line) curves 2 are approximating data

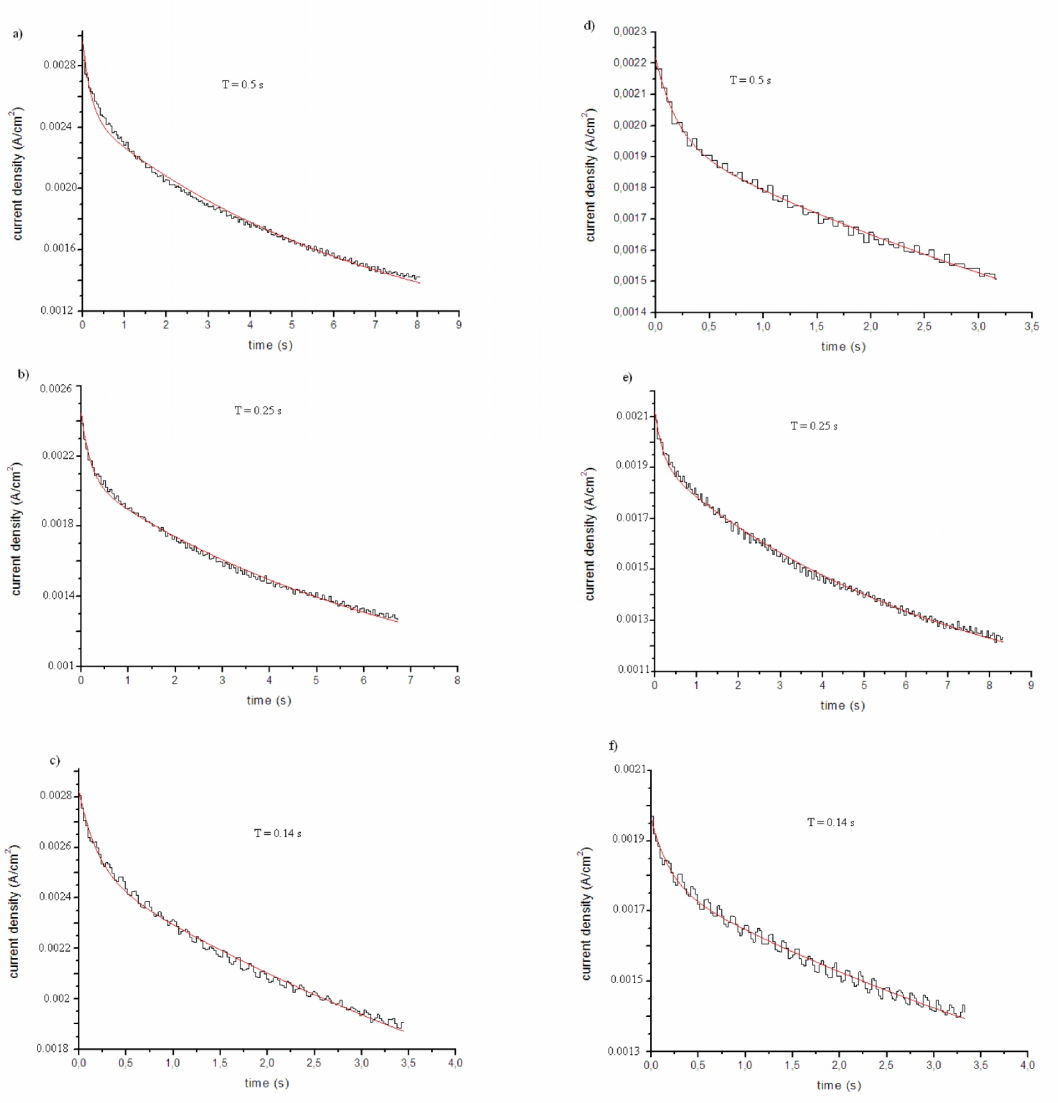

Fig 11. Approximation of relaxation parts of photocurrent pulses in sample 3 (the light is off after short lighting): a), b), c) experiment without filter; d), e), f) experiment with UVL-1 filter; noisy curves are experimental, red (color on-line) smooth curves are approximating data

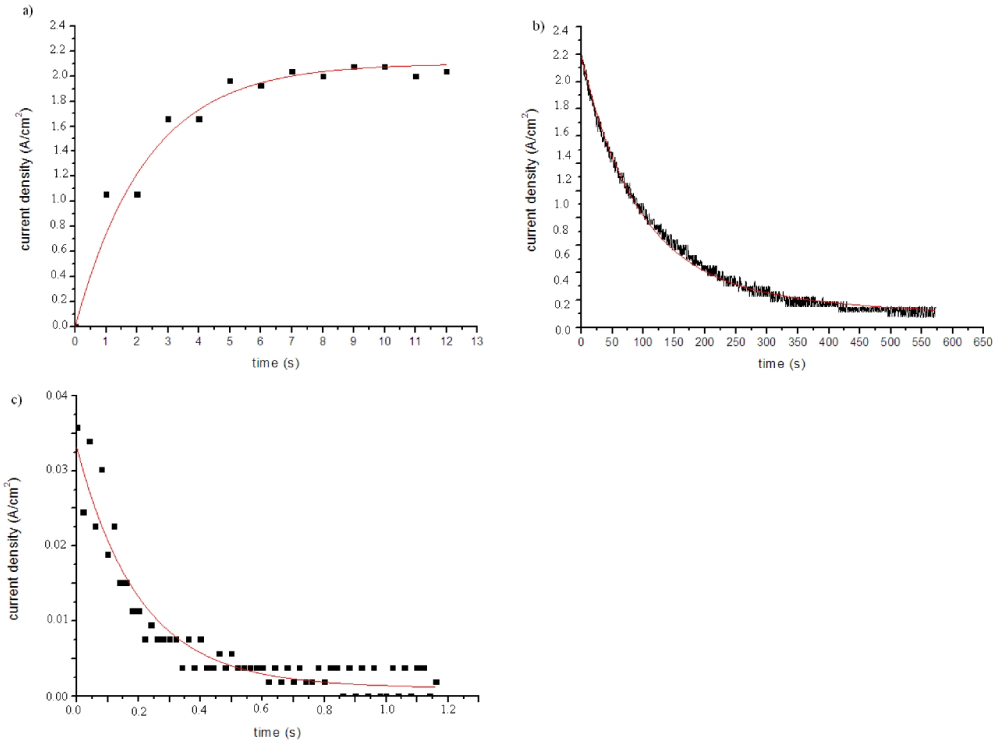

Fig. 12. Relaxation processes in sample 4: a) photocurrent buildup (the light is on)); b) relaxation part (the lamp is not switched off); c) relaxation part (the lamp is switched off); red (color on-line) smooth curves are the approximating functions

4.3. Photoconductivity on Laser Excitation

The shortest characteristic time of the relaxation processes observed in the above mentioned experiments with TiO_2 films was 0.02 s. There evidently exist faster processes. For example, the authors of [9] described relaxation processes with characteristic times of order picoseconds.

For determining the relaxation times in our experiments we considered photocurrent pulses arising at short-term sample exposure to light for 0.5 s, 0.25 s and 0.14 s. For recording faster relaxation processes, shorter excitation pulses are demanded. Shorter pulses are generated by a pulse laser, e.g., operating in the Q-switched mode. It is also important that the laser radiation wavelength should be either about 265 nm or about 310 nm, as sample sensitivity is highest at these wavelengths.

The experiment was carried out with a solid yttrium aluminate laser with the wavelength λ =1079.6 nm. For generation of radiation in the required frequency range the laser radiation frequency was first converted to the second and then to the fourth harmonic. As a result the sample was illuminated at the wavelength $\lambda = 269.9$ nm. The average radiation power at the fourth harmonic was 0.9 mW, pulse duration 10 ns, repetition rate 12.5 Hz. We did not observe single photoconductivity pulses at such parameters, as was done in [20,21], but we

observed accumulated photocurrent analogous to the case of continuous illumination. This effect is explained by the fact that the energy of a single pulse is insufficient for recording a single photoconductivity pulse, but averaged excitation is accumulated due to a high pulse repetition rate.

We also conducted experiments on detecting photoconductivity at the third harmonic of YAG: Nd+3 laser (pulse repetition rate 2 Hz, λ =355 nm, energy in a 10 ns pulse ≈0.4 mJ). Under these conditions, photoconductivity was not detected in the samples. This result corresponds to data of spectral measurements of absorption (λ = 355 nm corresponds to the edge of the absorption band (see Fig. 1) and to the photoconductivity spectrum (see Sec. 3.2 for detail).

Results of the experiment with sample 4 are presented in Fig. 13. Like in the previous experiments, the time dependence of photocurrent has extremum. The characteristic times of relaxation processes found by the building up part of the time dependence of photocurrent are the following: τ_1 = 600 s; τ_2 = 90 s.

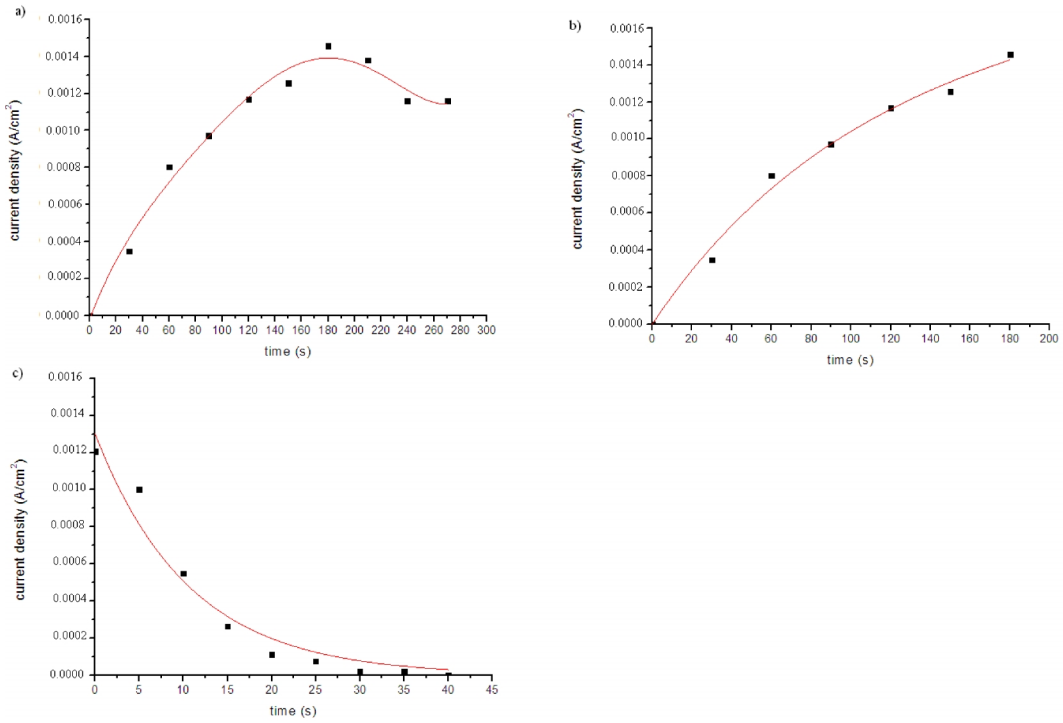

Fig. 13. Experiment with laser excitation. Sample 4: a) photocurrent *versus* time under continuous exposure; b) approximation of the building up part of the dependence; c) approximation of photocurrent relaxation after illumination is switched off. Red (color on-line) smooth curves are the approximating functions

The time constant calculated by the photocurrent relaxation on switching off sample illumination is τ_3 = 10 s.

The obtained values differ from the results of the previous experiments. Different relaxation mechanisms are, evidently, triggered when carriers are excited by a narrow band source. Obviously, when carriers are excited by a narrow band source to higher energy states, the relaxation mechanisms differ from those in the case of excitation of broadband radiation primarily to lower states.

4.4 Spectral Dependence of the Sensitivity of Sample Photoconductivity

Samples 3 and 4 are regarded to be most interesting for further consideration as the photoconductivity effect is much more pronounced in these samples. These samples were fabricated by similar technologies, but they have different time dependences of photocurrent. To clarify the cause of the difference between these samples we measured their spectral sensitivity.

We define sample sensitivity as a coefficient between the sample response (measured photocurrent) and radiation intensity at a given wavelength:

$$\alpha_{(\lambda)} = \frac{j}{I_{\lambda}} , \tag{3}$$

where $\alpha_{(\lambda)}$ is sensitivity, j is current density, and I_{λ} is radiation intensity at a given wavelength.

For measuring $\alpha_{(\lambda)}$ the current values of photocurrent were normalized to the maximum value in the photocurrent spectrum and to relative intensity of separate emission lines of the mercury lamp PRK-4 whose light intensity distribution in wavelengths is known [22]. Individual spectral lines of the lamp were extracted by means of the monochromator MDR-2. The absolute magnitude of sensitivity $\alpha_{(\lambda)}$ was determined by laser radiation measurements at the wavelength of 270 nm described above.

Spectral sensitivity of the studied samples is illustrated in Fig. 14. Clearly, each sample has two characteristic peaks where sensitivity increases. They correspond approximately to the same values of wavelengths. In different samples they differ only by the peak intensity ratio and by integral full-spectrum value, in conformity with the value of sensitivity when a full spectrum of the lamp is used. It is also clear that the photoconductivity effect is actually caused by two sections of the spectrum, one in the region of 265 nm, and the other in the region of 310 nm.

The presence of two sensitivity peaks with different magnitudes of sensitivity is evidently due to the zone structure of the film. Perhaps, this is concerned with direct and indirect transitions, or with splitting of the conductivity zone.

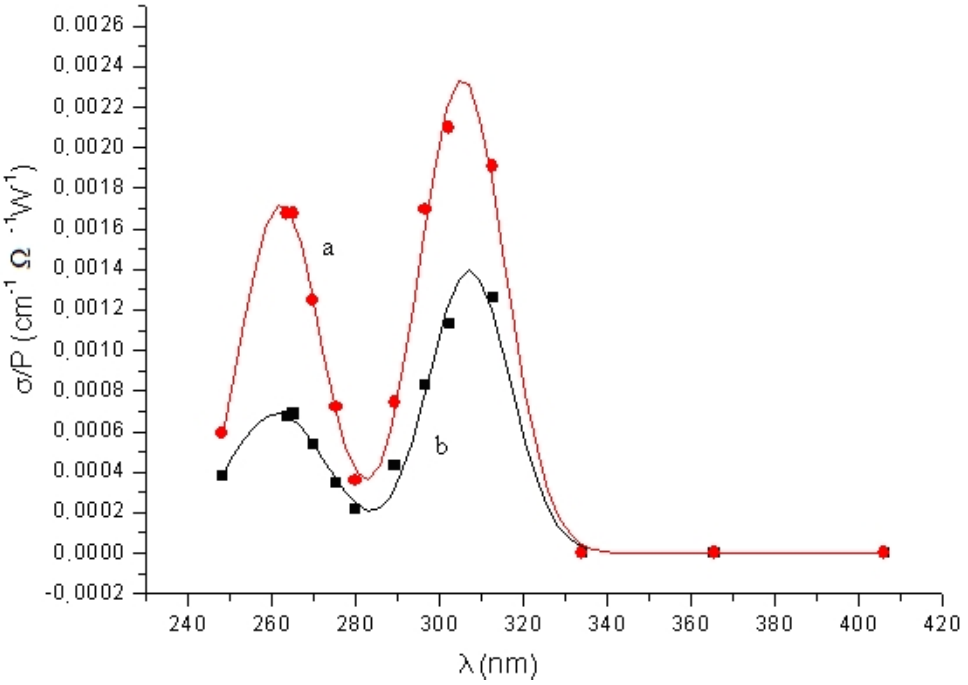

Fig. 14. Spectrum of photoconductivity sensitivity of samples 3 and 4 – ratio of sample conductivity σ ($\Omega^{-1}\cdot cm^{-1}$) to radiation power P (W/cm^2). Red (color on- line) curve a is sensitivity spectrum of sample 3, curve b is sensitivity spectrum of sample 4

5. DISCUSSION OF THE RESULTS

5.1 General Results

In the present work we obtained experimentally and studied various regimes of photoconductivity for different experimental samples of TiO_2 films. The results of this work are listed in Table 1.

5.2 Kinetics of Current Photocarriers

The data in Table 1 demonstrate the most interesting result of our work – multirelaxational character of photoconductivity kinetics, with characteristic relaxation times differing by orders of magnitude.

Table 1. The regimes of photoconductivity and typical photoconductivity relaxation times for some experimental samples of TiO_2 films. Two values with the label* are given for the experiment with a lamp and for the experiment with a laser (in brackets)

Sample	Type of film	Photoconductivity regime	Characteristic times of relaxation processes (s)				
			τ_1	τ_2	τ_3	τ_4	τ_5
1	Thickness 80 nm, nonannealed	Photoconductivity is observed, but the effect is very weak	Not measured				
2	Thickness 40 nm, annealed at 450 ^{0}C	Photoconductivity is due to surface activity	Photoconductivity is fully relaxed in 1 min				
3	Thickness 80 nm, annealed at 450 ^{0}C	Pronounced photoconductivity effect, the process saturates	625 (build up)	72 (build up)	7 (build up, relaxation)	0.2 (relaxation)	0.02 (relaxation)
4	Thickness 80 nm, annealed at 450 ^{0}C, deposited on silica glass	Pronounced photoconductivity effect, process with extremum	* 2.3 (build up, relaxation) (10, build up)	0.02 (build up, relaxation)		90 (relaxation, lamp is on)	600 (relaxation, lamp is on)
5	Thickness 80 nm, annealed at 520 ^{0}C	Photoconductivity effect is weak, buildup and relaxation times greatly exceed analogous times for samples 3 and 4	Very slow buildup times (about an hour) and still slower photoconductivity relaxation times (about several hours)				

An interpretation of the kinetics of internal photoeffect in thin TiO_2 films was proposed in [8]. According to this work, the time dependence of photocurrent concentration may be described assuming that the contribution to conductivity of free holes is small compared to that of electrons whose mobility does not depend on their concentration, only deep traps are considered, and electrons are immediately trapped in them. Numerical analysis of this model presented in [8] shows that, depending on the model parameters ratio (concentration of traps,coefficient of electron trapping, and coefficient of interband recombination), there may exist solutions for the time dependence of photocurrent both with saturation and with maximum and subsequent decay, which agrees upon the whole with the experimental results considered above. Moreover, from the data obtained in one of the experiments in [8] one can find linear recombination time τ_1 = 7.1 s that coincides with one of the relaxation time τ_3 = 7 s in the experiments with sample 3 (with saturation dependence). However, some aspects of our research, multirelaxational character of kinetic dependences with relaxation times differing by several orders of magnitude, in the first place, cannot be described by the model proposed in [8]. It is most likely due to the presence of several types of traps, with trapping coefficients and lifetimes differing by orders of magnitude and caused by different types of defects, for example, borders of crystallites of different types, crystallite-pore, crystallite-substrate and crystallite-air borders. Relaxation times differ for different samples also. More exact interpretation demands further studies.

The fact that different photoconductivity regimes are observed for two samples with identical parameters (samples 3 and 4) is of great interest. The photoconductivity in sample 3 is cumulative, eventually going to a stationary regime, whereas in sample 4 it has an extreme character, it reaches a maximum under continuous illumination after which it relaxes almost to zero. Spectral dependence of photoconducting films is almost the same, but the absolute magnitude of photoconductivity of sample 3 is twice that of sample 4. Different behavior, relaxation times, and sensitivity are the result of different internal structure of the samples and, most probably, unstable technique of film deposition. The impact of film thickness on photoconductivity (sample 2) is quite distinct, although film 2 was annealed in the same regime as films 3 and 4. This may be attributed to the influence of surface structure of the substrate on the structure of the first adjacent layer (40 nm) of the thin film that acts as a buffer. In addition, substrate microroughness exceeding 4 nm may also affect the structure of the first layer. It is necessary to understand in the future research drift of which parameters (annealing temperature, film thickness, solution purity) in the course of fabrication affects the final result, which will allow controlling them more rigorously. On the other hand, it is quite possible that different photoconductivity regimes may be useful for different applications. Hence, it is necessary to learn within the framework of the available technology to produce films with a preset photoconductivity regime by rigorously controlling parameters of the technological process.

The photoconductivity in sample 5 is much weaker than in its twin sample 4. This may be attributed to the conversion of the film from anatase to rutile at temperatures exceeding 500 ºC [15,23].

The difference between the relaxation times in sample 4 obtained in experiments with a lamp and a laser is worthy of notice. This may be caused by the difference in the carrier relaxation at narrowband and broadband excitation. Also of interest is an extremely broad “window” in the characteristic lifetimes of free and trapped carriers (from 10^{-11} s to 10^{-2} s). Existence of transition processes with times in this “window“ is still to be understood.

5.3 Spectral Dependence

Let us consider again spectral sensitivity of the samples. Assuming that the spectral dependence of photoconductivity is determined primarily by absorption spectrum, using the method of determining a forbidden gap by the self-absorption edge it is possible to find a forbidden gap for the samples. According to this method, the forbidden gap is found from the dependence of absorption coefficient α on the energy of a quantum ε (e.g., in electron-volts). For direct transitions, the forbidden gap is determined by the linear part of the dependence of squared absorption coefficient α^2 on frequency, for forbidden direct transitions by the dependence of absorption coefficient to the power of 2/3, and for forbidden indirect transitions by the dependence of α on frequency to the power of 2 [10]. For determining a forbidden gap the linear part of the dependence is extrapolated by a straight line and the forbidden gap corresponds to the intersection of the frequency axis.

The edge of the photoconductivity spectrum (Fig. 13) was insufficiently robust for accurate assessing of the forbidden gap E_g. However, we can state that the value of the first, low-frequency band edge is 3.72 eV ≤ E_{g1} ≤ 3.96 eV, which agrees with the value of E_g obtained from the absorption spectra. For the second, high-frequency band edge we have 4.4 eV ≤ E_{g2} ≤ 4.5 eV.

There is a controversy in the literature concerning the magnitude and type of forbidden gap. The magnitude of forbidden gap E_g ≈ 3.7 eV presented in our work for the absorption band edge and photoconductivity evidently corresponds to the magnitude predicted theoretically for direct transitions in [24] for anatase crystals (E_g = 3.45 eV or 3.59 eV, depending on polarization). A slightly larger value of E_g obtained in our work may be attributed to “blue shift” of the absorption band in nanosize films [25] as well as to indefiniteness in measurements caused by the interference of light in the film. The magnitude of the absorption coefficient in the region ε ≥ 3.7 eV (Fig. 19) also corresponds to direct transitions. This identification of the direct forbidden gap is also found by other researchers, see for example [26, 27], whereas in some other works [28] the band gap E_g ≈ 3 eV is regarded to be a direct transition. Our data indicate that the lower direct gap is E_g ≈ 3.7 eV. The transitions corresponding to the absorption in a longer-wave spectral region with the edge ~ 3 eV most likely correspond to indirect transitions [23]; they were not observed in our work because of their relative weakness and small film thickness. The gap E_g ≈ 4.5 eV in the photoconductivity spectra measured in this work is also likely to correspond to direct transitions (judging by the magnitude of the effect), possibly to E_g = 4.3 eV ($\Gamma_2 \rightarrow \Gamma_1$) and E_g = 4.8 eV ($\Gamma_3 \rightarrow \Gamma_5$) according to [24].

6. CONCLUSION

1. Different photoconductivity regimes for samples of thin titanium oxide films of different thicknesses and phase states produced by the sol-gel technique have been obtained.
2. A multirelaxion character of processes of photoconductivity onset with relaxation times differing by several orders of magnitude has been revealed.
3. Spectral features of the photoconductivity effect have been ascertained. The dependences of sample sensitivity on radiation source wavelength have been found. The corresponding curves have pronounced maxima at about 265 nm and 310 nm.
4. Magnitudes of the forbidden gap have been assessed by transmission spectra of the films and by spectral sensitivity of the photoconductivity. According to the data of

optical measurements, the forbidden gap is ≈ 3.7 ÷ 3.8 eV; according to the data of photoelectric measurements for the main sensitivity peak, the forbidden gap is also ≈3.7 eV, and for the second peak it is 4.5 eV.

Summing up the results of our work we can draw the following conclusions: Current carriers generated during interband transition are rapidly (with about picosecond lifetime) trapped by long-lived (10^{-2} – 10^{2} s) traps, where they are accumulated and redistributed on the energy ladder, the steps of which correspond to different types of traps with different lifetimes. Escaping from these traps the carriers produce conductivity that

a) is cumulative with a characteristic time corresponding to maximum lifetime of the traps, and
b) decays in a multirelaxation manner after the end of irradiation with characteristic times corresponding to lifetimes of the most efficient steps of the ladder of traps.

It is quite possible that different types of traps (steps of the ladder of traps) correspond to different types of mesoporous film borders. Of particular interest is an extremely wide "window" in the characteristic lifetimes of free and trapped carriers (from 10^{-11} s to 10^{-2} s). The existence of transition processes with the times inside this window needs further investigation.

ACKNOWLEDGEMENTS

The authors are grateful for partial financial support received from RFBR (Grant No. 12-02-01075-a), the Program of the Presidium of the Russian Academy of Sciences "Fundamentals of nanostructure and nanomaterial technologies" and State Contract No. 14.513.11.0081 with RF Ministry of Education and Science. The authors appreciate useful discussions with N.Bityurin.

COMPETING INTERESTS

The authors declare that there are no competing interests.

REFERENCES

1. Miyauchi M, Nakajima A, Watanabe T, et al. Photocatalysis and photoinduced hydrophilicity of various metal oxide thin films. Chem. Mater. 2000;14:2812.
2. Pleskova SN, Golubeva IS, Verevkin Yu K, Pershin EA, Burenina VN, Korolikhin VV. Photoinduced bactericidal activity of TiO_2 films. Applied Biochemistry and Microbiology. 2011;47:28. Russian.
3. Pleskova SN, Golubeva IS, Verevkin Yu K. Dynamics of the TiO_2 nanofilms bactericidal activity. J Environ Occup Sci. 2012;1(2):71.
4. Liu Hou W, Hsuan W, Pavaskar P, Cronin SB. Plasmon Resonant Enhancement of Photocatalytic Water Splitting Under Visible Illumination Nano Lett. 2011;11:1111.
5. Takeuchi M, Sakamoto K, Martra G, Coluccia S, Anpo M. Mechanism of photoinduced superhydrophilicity on the TiO_2 photocatalyst surface. J Phys Chem B. 2005;109(32):15422.
6. Pil Tai Weon-, Oh Jae-Yee. Fabrication and humidity sensing properties of nanostructured TiO_2-SnO_2 thin films. Sensors and Actuatos *B.* 2002;85:154.

7. Vomvas A, Pomoni K, Tarapalis C, Todorova N. Photoconductivity in sol-gel TiO_2 thin films with and without ammonia treatment. Materials Science-Poland. 2007;25:809.
8. Zavyalov AV, Shapovalov VI, Shutova NS. Kinetics of the internal photoelectric effect in films of titanium oxide. Technical Phys. Lett. 2011;37:1008.
9. Němec H, Kužel P, Kadlec F, Fattakhova-Rohlfing D, Szeifert J, Bein T, Kalousek V, Rathouský J. Ultrafast terahertz photoconductivity in nanocrystalline mesoporous TiO_2 films. Applied Physics Letters. 2010;96:062103.
10. Chen CH, Shieh J, Hsieh SM, Kuo CL, Liao HY. Architecture, optical absorption, and photocurrent response of oxygen-deficient mixed-phase titania nanostructures. Acta Materialia. 2012;60:6429.
11. Xia XH, Lu L, Walton AS, Ward M, Han XP, Brydson R, Luo, JK, Shao G. Origin of significant visible-light absorption properties of Mn-doped TiO_2 thin films. Acta Materialia. 2012;60:1974.
12. Nicula R, Stir M, Schick C, Burkel E. High-temperature high-pressure crystallization and sintering behavior of brookite-free nanostructured titanium dioxide: in situ experiments using synchrotron radiation Thermochimica Acta. 2003;403(1):129.
13. Hartmann P, Lee DK, Smarsly BM, Janek J. Mesoporous TiO_2: Comparison of Classical Sol-Gel and Nanoparticle Based Photoelectrodes for the WaterSplitting Reaction. Available: www.acsnano.org. 2010;4 3147-3154.
14. Maksimov AI, Moshnikov VA, Taitov Yu M, Shilova OA. Fundamentals of the Sol-Gel technology of Nanocomposites, St-Petersburg Electrotechnical University; 2007 (in Russian).
15. Suikovskaya NV. Chemical Methods of Obtaining Thin Transparent Films, Chemistry, Chemistry, Leningrad; 1971. Russian.
16. Danilin BS, Syrchin VK. Magnetron Sputtering Systems, Radio i Svyaz, Mocsow; 1982. Russian.
17. Chemical Vapour Deposition. Precursors, Processes and Application, Eds. A.C. Jones, M.L. Hitchman, London: RSC Publishing, 2009.
18. Tolstikhina AL, Sorokina KL. Structural features of amorphous titanium oxide films depending on the preparation conditions. Crystallography. 1996;41:339. Russian.
19. Titanium dioxide. Available: http://en.wikipedia.org/wiki/Titanium_dioxide.
20. Bredikhin VI, Genkin VN, Soustov LV. Photoconductivity of Semiinsulating GaAs Under Strong Excitation Conditions. Soviet Physics-Semiconductors. 1976;10:726. Russian.
21. Bredikhin VI, Genkin VN, Miller AM, Soustov LV. Photoelectric effects in KDP and DKDP crystals subjected to laser radiation. Zh. Eksp. Teor. Fi. 1978;75:1763.
22. Bozhevolnov EA. Luminescent Analysis of Inorganic Susbances, Chemistry, Moscow 1966;15pp. (in Russian).
    Available: http://www.ngpedia.ru/pngs/070/070jLzF7U7b602n5a2T6.png
23. PY, Yu, M. Cardona. Fundamentals of Semiconductors Physics and Materials Properties, 3rd ed.; Springer: Berlin,Heidelberg, New York. 2005;268-276..
24. Daude N, Gout C, Jouanin C. Electronic band structure of titanium dioxide. Physical Review B. 1977;15:3229.
25. Manorama AR. Reddy. Bandgap studies on anatase titanium dioxide nanoparticles. Materials Chemistry and Physics. 2003;78:235.
26. Valencia S, Marín JM, Restrepo G. Study of the Bandgap of Synthesized Titanium Dioxide Nanoparticules Using the Sol-Gel Method and a Hydrothermal Treatment. Materials Letters. 1995;25:l-275. Available:
    http://www.benthamscience.com/open/tomsj/articles/V004/SI0001TOMSJ/9TOMSJ.pdf

27. Sakulkhaemaruethai S, Pavasupree S, Suzuki Y, Yoshikawa S. Photocatalytic activity of titania nanocrystals prepared by surfactant-assisted templating method—Effect of calcination conditions. Materials Letters. 2005;59:2965.
28. Sanchez E, Lopez T. Effect of the preparation method on the band gap of titania and platinum-titania sol-gel materials. Materials Letters. 1995;25:271.27. K.M. Reddy, S.V.

Peer-review history:
The peer review history for this paper can be accessed here:
http://www.sciencedomain.org/review-history.php?iid=224&id=4&aid=1812